

This document was prepared in conjunction with work accomplished under Contract No. DE-AC09-96SR18500 with the U.S. Department of Energy.

DISCLAIMER

This report was prepared as an account of work sponsored by an agency of the United States Government. Neither the United States Government nor any agency thereof, nor any of their employees, makes any warranty, express or implied, or assumes any legal liability or responsibility for the accuracy, completeness, or usefulness of any information, apparatus, product or process disclosed, or represents that its use would not infringe privately owned rights. Reference herein to any specific commercial product, process or service by trade name, trademark, manufacturer, or otherwise does not necessarily constitute or imply its endorsement, recommendation, or favoring by the United States Government or any agency thereof. The views and opinions of authors expressed herein do not necessarily state or reflect those of the United States Government or any agency thereof.

This report has been reproduced directly from the best available copy.

Available for sale to the public, in paper, from: U.S. Department of Commerce, National Technical Information Service, 5285 Port Royal Road, Springfield, VA 22161

phone: (800) 553-6847

fax: (703) 605-6900

email: orders@ntis.fedworld.gov

online ordering: <http://www.ntis.gov/support/index.html>

Available electronically at <http://www.doe.gov/bridge>

Available for a processing fee to U.S. Department of Energy and its contractors, in paper, from: U.S. Department of Energy, Office of Scientific and Technical Information, P.O. Box 62, Oak Ridge, TN 37831-0062

phone: (865)576-8401

fax: (865)576-5728

email: reports@adonis.osti.gov

Performance analysis of conical cavities for surface temperature retrieval with a Fourier transform infrared spectrometer

Eliel Villa-Aleman
Savannah River Technology Center, Aiken, SC 29808

ABSTRACT

The Savannah River Technology Center (SRTC) is conducting measurements in the visible, near-infrared and infrared spectral regions of selected ground targets in support to the Department of Energy Multispectral Thermal Imager (MTI) satellite. Radiometers have been used to retrieve surface temperature from water and land targets. Surface temperature measurements of land targets are often complicated by the wavelength dependent emissivity. Conical cavities have been employed on land targets to increase the surface effective emissivity and therefore the apparent surface temperature. Surface effective emissivity values near unity offer the opportunity for absolute surface temperature retrieval. The efficacy of conical cavities for absolute surface temperature retrievals was studied with a calibrated Fourier transform infrared spectrometer (FTIR). The research paper presents the results of surface temperature retrievals of targets with low emissivity values with the aid of conical cavities.

Keywords: MTI satellite, temperature measurements, FTIR

Introduction

The relentless interest in ground surface temperature retrieval by the scientific community using satellites such as MTI and ASTER and other airborne sensors requires accurate ground truth temperature measurements. Surface temperature measurements can be subdivided into two main categories: water and soil targets. Water surface temperatures are influenced by the skin temperature effect. The skin temperature measured by a satellite is within the upper 1mm layer and is typically 0.2 – 1.0 C below the bulk water temperature (uppermost 10 cm), deviations larger than 1C are not uncommon.

In contrast to water targets with high emissivity values and smooth gradual spectral variation (emissivity ~ 0.986 @ 14 μ m), many soil targets have large variations in their spectral emissivity. Radiometers are often used to measure apparent surface temperature of targets. Poor knowledge of the soil spectral emissivity can result in a poor characterization of the true temperature of the target surface. Contact thermocouples have also been used to measure surface temperature with mixed results. Contact thermocouples errors primarily result from poor contact and their effect on the energy balance with the environment.

Several methods have been presented in the literature to measure target surface temperatures with a broad band radiometer. Fuchs and Tanner^{1,2} demonstrated the use of a highly reflective aluminum cone in conjunction with an infrared radiometer in their pursuit to measure surface temperatures. The highly reflective aluminum cone was used to create a quasi “blackbody cavity” from a target surface. The aluminum cone blackbody cavity concept is an extrapolation to the blackbody approximation of a pierced hole in an isothermal cavity. Lightfoot³, Chandos⁴ and others have showed the blackbody approximation by a pierced hole in an isothermal and diffuse cavity. Chandos et. al. derived the performance of several cavities including spherical cavities responsible for equation 1. The effective emissivity of the hole in the diffuse isothermal cavity is described by equation 1 where $\epsilon_{\text{material}}$ is the cavity emissivity, A_h is the area of the hole and R_s is the radius of the sphere.

$$\epsilon_{\text{effective}} = \frac{\epsilon_{\text{material}}}{\epsilon_{\text{material}} + \frac{A_h}{4\pi R_s^2} (1 - \epsilon_{\text{material}})} \quad (1)$$

Fuchs and Tanner used a variant of equation 1 by replacing the $\frac{A_h}{4\pi R_s^2}$ term in equation 1 with the ratio of the cone apex and base areas ($RA = A_{apex}/A_{base}$) as shown in equation 2.

$$\mathcal{E}_{theoretical-effective} = \frac{\mathcal{E}_{material}}{\mathcal{E}_{material} + \frac{A_{apex}}{A_{base}}(1 - \mathcal{E}_{material})} \quad (2)$$

The effective emissivity in equation 2 approaches unity (blackbody) at the limit where the ratio RA approaches zero. In this ideal case, Fuch and Tanner reasoned that a conical cavity with an infinitely small apex/base area ratio, on top of a target, could approximate a blackbody target. The target band emissivity can then be measured as shown in equation 3 where L_{target} , $L_{background}$, and L_{target_cone} are the measured radiances of the target, background and the target with a conical cavity respectively.

$$\mathcal{E}_{band} = \frac{L_{target} - L_{background}}{L_{target_cone} - L_{background}} \quad (3)$$

Equation 3 was approximated by using the temperature equivalent radiance terms as shown in equation 4.

$$\mathcal{E}_{band} = \frac{T_{target}^4 - T_{background}^4}{T_{target_cone}^4 - T_{background}^4} \quad (4)$$

The temperatures measured with and without the cone in conjunction with the background temperature using an infragold plate (or crinkled aluminum foil) can be used to estimate a band-integrated emissivity of the target. The deviation in the band emissivity calculated using equation 4 from the true band emissivity is primarily due to the deviation in the temperature measurement of the target $T_{target-cone}$. Since the cone walls are not perfectly reflective ($\epsilon > 0$), small fraction of energy emitted by the target is lost to the cone walls. Therefore, the cone cavity formed from the cone walls at temperature T_1 and the target at a temperature T_2 does not represent an isothermal cavity. The deviation in the target temperature measurement using a conical cavity from the true temperature is expected to increase with the temperature difference between the wall and the target. Although temperature deviations are expected using the conical cavity method, the method is accurate, simple and easy to apply to the measurement of temperature and emissivity of a target with high emissivity and near ambient temperatures. SRTC has used the cone's method to measure temperature on concrete and asphalt surfaces.

In order to establish the validity of temperature and emissivity measurements with the cone, a series of experiments were conducted in the laboratory with an aluminum plate coated with a known spectral emissivity paint and a calibrated Fourier transform infrared spectrometer. The performance of several conical cavities with different RA ratios (conebase, cone C, cone B, cone A and metal cone) was tested using a heated-target painted with highly variable wavelength dependent emissivity coating. An infrared camera was also used to measure the apparent temperature of the target with and without the cone.

The present assessment study identified discrepancies between the theoretical and experimental effective emissivities except for targets with large emissivity values or targets at similar temperatures to the cone's wall temperature. Equation 2 was modified (equation 10) to take into account the temperature differences between the cone and the target. The modified semi-empirical formula was shown to closely follow the wavelength dependent experimental effective target emissivity.

2. EXPERIMENTAL

The performance of the conical cavities was conducted with a heated aluminum plate coated with a low-emissivity paint. The low-emissivity coating is a special paint manufactured by Chemrex called Radiance Low-e Attic and Decking Radiant Barrier. The emissivity of the paint is wavelength dependent with a minimum of 0.42 at 5.36 μm . The temperature of the target with dimensions of 25.4cm x 25.4cm x 0.635cm was controlled with a heating blanket. The temperature of the target was monitored with a tubular insertion thermistor probe and also a surface temperature thermocouple. The surface temperature was 1.5C cooler than the respective insertion probe for experiments without the cone. The temperature difference decreased to 0.6C for experiments with the cone placed on top of the contact thermocouple. The temperature discrepancy is reasonable due to convection and radiative losses. Figure 1 shows the heated aluminum plate with the FTIR setup for the cone experiments.

Several conical cavity sizes (same base area with different apex areas) were used in this study (conebase, cone C, cone B, and cone A). The base/apex diameters of the cone were modified using a "base" cone with a "modifier" cone. The "base" cone is a stainless steel cone with the inner wall covered with aluminum tape. The emissivity of aluminum foil is 0.04. Previous experiments have shown the aluminum tape with a higher emissivity than the foil. The "modifier" cones were made out of cardboard. The inner wall also covered with aluminum tape. The "modifier" cones were set on top of the conebase to modify the area of the conical cavity apex. The apex area (at a constant base area) was only changed during the course of the experiment. An aluminum foil cone and a metal and heated metal cones were also tested during the course of the experiment. Table 1 shows the dimensions of the cones used during the course of the experiment.

Infrared imaging studies were conducted with an infrared camera manufactured by Inframetrics (model SC2000). The apparent temperatures of the target with and without the conical cavity were analyzed with the infrared camera. Prior to temperature measurements, the imaging infrared radiometer was calibrated using a blackbody manufactured by MIKRON Corporation (model M340). The blackbody has an accuracy of 0.2C.

A Fourier transform infrared spectrometer (FTIR), manufactured by Midac Corporation (M2400 series, the illuminator), was used to measure wavelength dependent radiance of the target and its spectral emissivity. The spectrometer has a 3.8cm aperture diameter with a 40 milliradians field of view (FOV). The spectrometer was equipped with mercury cadmium telluride (MCT) detector cooled with liquid nitrogen to 77K. The temperature of the spectrometer was stabilized using a heated insulated jacket. The housing of the FTIR spectrometer was maintained at 40C with the aid of heating blankets and an insulated jacket. Heating blankets were placed above and below the FTIR. The heating blankets attached to the FTIR spectrometer were insulated from the ambient air with Styrofoam sheets and an aluminum shield. A thermocouple was attached to the FTIR spectrometer housing for temperature monitoring and control. The temperature controller maintained the FTIR spectrometer temperature within 0.2C of the selected temperature. The instrument was warmed-up for 1½ hours prior to data acquisition.

The FTIR spectrometer was assembled on an optical table. The FTIR spectrometer window entrance was 21" from the target surface. A platform with a steering beam mirror made out of stainless steel rods was attached to the FTIR spectrometer front surface. A gold-coated off-axis parabolic mirror was used to steer the target radiance into the spectrometer.

Calibration of the FTIR spectrometer was accomplished through the use of a MIKRON blackbody model M340 at four different temperatures. The temperature of the blackbody was set at 55, 45, 35, and 25C. The air temperature in the laboratory was approximately 21C during the course of the experiment. One hundred twenty eight spectra were co-added during the target, blackbody and laboratory background measurements. The laboratory background was measured with a diffuse infragold-coated plate manufactured by Labsphere. The temperature of the infragold-coated plate was monitored with thermistor probes manufactured by Omega with 0.02C accuracy. The blackbody temperatures were accurate to 0.2C. The temperature of the heated and coated aluminum plate was monitored with a tubular digital thermometer and a contact surface thermocouple. The temperature of the contact thermocouple was always cooler than the temperature measured with the tubular thermometer. The temperature difference without any cones enclosing the contact thermocouple was ~1.0C. The temperature difference decreased upon the placing of the cone to about 0.6C. The temperature difference was primarily the result of convection, and conduction at the thermocouple junction. Thermal images of the thermocouple contact on the heated plate clearly identifies the cooling effect of the contact thermocouple junction.

The FTIR spectra were acquired by measuring raw spectra of the target, followed by conebase, cone c, cone b, cone a, aluminum foil cone, metal cone, and heated metal cone. The recorded spectra of the target with the cones were followed by measurements of the infragold (lab background) and the blackbody at the four temperatures. The instrument response function (IRF) was calculated from the blackbody measurements. The target and cones radiances and emissivities were calculated from the raw data and the IRF.

3. RESULTS AND DISCUSSION

The FTIR spectrometer was calibrated by calculating the instrument response function (IRF) with the aid of two blackbodies. The IRF was calculated as

$$IRF = \frac{BB_{Hot} - BB_{Cold}}{L_{Hot} - L_{Cold}}. \quad (5)$$

BB_{hot} and BB_{cold} are the raw machine unit spectra for the hot and cold blackbodies and L_{hot} and L_{cold} are the Planck distribution functions for the temperatures of the blackbodies. Once the IRF was calculated, the target radiance was calculated from

$$L_{target} = L_{Hot} - \frac{(BB_{Hot} - BB_{target})}{IRF} \quad (6)$$

The laboratory background was measured with a diffuse infragold-coated plate. The laboratory radiance was calculated from

$$L_{Laboratory} = L_{Hot} - \frac{(BB_{Hot} - BB_{Laboratory})}{IRF} - L(T)_{Gold_Plate} \quad (7)$$

The theoretical Planckian curve for the heated target plate was calculated using the temperature measured with the contact thermocouple and also with the tubular thermometer ($L_{target_theoretical}$). The calculated blackbody radiances at the contact and tubular temperatures in conjunction with the experimentally measured laboratory ($L_{Laboratory}$) and target radiances (L_{target}) were used to calculate the emissivity of the material as shown in in equation 8.

$$\varepsilon = \frac{(L_{target} - L_{Laboratory})}{(L_{target_theoretical} - L_{Laboratory})}. \quad (8)$$

The spectral effective emissivity was calculated by placing the cone over the plate and measuring the radiance exiting the cone ($L_{effective_target_cone}$). The effective emissivity was calculated as shown in equation 9.

$$\varepsilon_{experimental-effective} = \frac{(L_{effective_target_cone} - L_{Laboratory})}{(L_{target_theoretical} - L_{Laboratory})}. \quad (9)$$

Figure 2 shows the emissivity spectrum of the Radiance Low-e Attic and Decking Radiant Barrier product in the 2-16 μ m spectral region.. The spectrum is characterized by large spectral variations in the emissivity. The spectral variations provide the opportunity to study the performance of equation 2. Figure 3 shows the emissivity of the target material and the measured effective emissivity of the target with the conebase, cone C, cone B, and cone A in the 10 to 15 μ m spectral range. Figure 4 shows the target emissivity spectrum and the corresponding theoretical spectral effective emissivity for conebase, cone C and cone A using equation 2. The differences between figures 3 and 4 are large for the corresponding cone sets, i.e.

the difference for the theoretical and experimental emissivity for cone A is ~0.1. Therefore, the application of equation 2 to temperature measurements with aluminum cone is not completely valid.

A closer inspection to equation 2 reveals that the ratio RA ($A_{\text{apex}}/A_{\text{base}}$) is related to power losses through the opening of the cavity. The aluminum cone/target setup does not represent an isothermal cavity. Therefore, it is expected that the temperature difference between the aluminum cone and the target play an important role in the observed discrepancies between experimental and theoretical effective emissivity values. It can be shown that the experimental and theoretical emissivity values can be superimposed by changing the RA parameter. Therefore, equation 2 can be modified to accept a temperature dependent function to model the experimental effective cone emissivities. Equation 10 shows the effective emissivity with apex/base area and temperature dependent function $f(\lambda, T_{\text{cone}}, T_{\text{target}})$.

$$\epsilon_{\text{effective}} = \frac{\epsilon_{\text{material}}}{\epsilon_{\text{material}} + \left(\frac{A_{\text{apex}}}{A_{\text{base}}} + f(\lambda, T_{\text{cone}}, T_{\text{target}}) \right) (1 - \epsilon_{\text{material}})} \quad (10)$$

The proper functionality of the $f(\lambda, T_{\text{cone}}, T_{\text{target}})$ function should include the configuration geometry factors for two gray disks (target at the base of the cone and apex of the cone) and the frustrum of the cone. The calculation of the heat transfer among the three surfaces and the net heat loss is a lengthy process. A simple approximation to the two disks and frustrum problem can be accomplished using the infinite gray parallel plates model with $\epsilon(\lambda)$ for the target and $\epsilon_{\text{aluminum}}$ for the cone. This approximation does not take into account the conduction between the rim of the cone and the target, and convection effects. In this approximation, the cone is projected into a disk with a hole in a center and with an area of the cone's frustrum. Also, in this approximation the target area is defined as the difference between the conebase and cone apex areas. The heat transfer model for infinite gray parallel plates is shown in equation 11 where $M(T_{\text{target}})$ and $M(T_{\text{cone}})$ are the spectral exitances at their respective target and cone temperatures.

$$\frac{\phi_{\text{target} \rightarrow \text{cone}}}{A} = \frac{M(\lambda, T_{\text{target}}) - M(\lambda, T_{\text{cone}})}{\frac{1}{\epsilon(\lambda)_{\text{target}}} + \frac{1}{\epsilon_{\text{cone}}} - 1} \quad (11)$$

The modifier $f(\lambda, T_{\text{cone}}, T_{\text{target}})$ is defined in equation 12 where the parallel plate model was modified by the areas of the frustrum, base and apex.

$$f(\lambda, T_{\text{cone}}, T_{\text{target}}) = \frac{M(\lambda, T_{\text{target}}) - M(\lambda, T_{\text{cone}})}{\frac{1}{\epsilon(\lambda)_{\text{target}}} + \frac{1}{\epsilon_{\text{cone}}} - 1} * \frac{A_{\text{frustrum}}}{(A_{\text{cone base}} - A_{\text{cone apex}})} \quad (12)$$

The cone temperature in equation 12 was set at the laboratory temperature, and the aluminum emissivity was set to 0.09. The beauty of the semi-empirical formula for the calculation of effective target emissivity is based on its simplicity. Figures 5a, 5b, and 5c show the target emissivity, the experimental cone effective emissivity and the performance with the calculated effective emissivities using equation 2 and the modified equation 10 for the conebase, cone C and cone A. The effective emissivities calculated using equation 2 overestimated the experimental effective emissivity values. The emissivity differences between the equation 2 values and the experimental values were in the order of 0.1. The effective emissivity values calculated using the modified version in equation 10 approximate the experimental results within 0.03. Most of the deviations between the modified version and the experimental effective emissivities in Figure 5a, 5b, and 5c are due to the approximation of the cone setup to a projected disk.

In the limit where the frustrum temperature equals the target temperature, the modified version (equation 10) approaches the results of equation 2. This case was tested using a metal cone with aluminum foil tape. The experiment was conducted by measuring the effective emissivity of the target with and without a heated metal cone. The temperature of the metal cone was monitored with a contact thermocouple and was accurate within 3 degrees. The temperature of the cone was heated to the temperature of the target. Figure 6 shows the results obtained with the ambient and heated metal cone. The dependence of the experimental effective emissivity on the cone's wall temperature was clearly demonstrated in this experiment and provides validity for the model with energy exchange between the target and the wall of the cone.

Analysis of the cone performance was also conducted using an infrared camera. The camera was positioned to see at the target plate and at the same location looking through cone base, cone A, cone B and cone C. Figure 7 shows the infrared images for the heated target, and the cone base, cone B and cone A. The temperatures measured with the radiometer shown in Figure 7 exceeds the true temperature by 0.8C. Table 2 shows the temperature of the calibrated radiometer. The apparent temperature difference between the contact thermocouple material and the target plate (47.8C versus 40.5C) is the result of the thermocouple material higher emissivity. The temperature of the target plate was measured with a tubular thermometer and a contact thermocouple. Convection and radiative effects for the target without a cone results in larger differences between the tubular and contact thermocouple temperatures. The tubular thermometer (50.25C) is ~1.3C higher than the corresponding contact thermocouple (48.9C). The temperature difference between the tubular thermometer and the contact thermocouple is reduced to ~0.7C for experiments with the cone. The calibrated radiometer temperature with cone A is 2.1C cooler than the corresponding contact thermocouple. The temperature difference between the contact thermocouple and the radiometer temperature is the result of the temperature difference between the target and the cone wall. The results with the infrared camera and the spectral emissivity measured with the FTIR spectrometer are mutually consistent.

Table 3 shows the results of a temperature dependence experiment. Temperatures of the target were measured with the tubular thermometer, contact thermocouple, and with the infrared camera (bare and through cone A). The temperatures were selected at ambient temperature and nominal temperatures of 30, 40, 50, and 60C. The data clearly shows the larger error associated with the temperature difference between the cone and the target.

SUMMARY

A Fourier transform infrared spectrometer was used to measure the spectral radiance of a target of known temperature. The FTIR was also used to measure the radiance of the target through the apex of cones with different apex and base areas. The emissivity of the target and the effective emissivity of a target with the cones of known apex and base areas were calculated from the spectral radiances. The theoretical effective emissivities for the cones used in the experimental setup were calculated using equation 2. Large discrepancies in the experimental and theoretical effective emissivities were measured (0.1) for a target and a cone at temperatures of 50C and 21C, respectively. The differences in effective emissivity between the theoretical and experimental values were traced to the temperature difference between the target and the cone. A modified model for the energy exchange between two infinite gray parallel plates at different temperatures was used to modify equation 2. The theoretical effective emissivities with equation 10 (modified equation 2) were shown to agree within 0.03 the experimental effective emissivity results.

An experiment was designed to test the effective emissivity dependence on the cone temperature. The effective emissivity was measured for a metal cone set at ambient and at the target temperatures. The effective emissivity measured with the cone at the target temperature was found to agree with the theoretical results calculated from a blackbody cavity (equation 2).

Infrared images of the target and the target with the cones with a broad band infrared camera (8-12 μ m) demonstrated a result similar to that obtained with the FTIR spectrometer. The temperatures measured with the radiometer were consistently lower than the temperatures measured with the tubular thermometer and contact thermocouple. Although the ratio RA of the cone A approached the dimensions for a blackbody cavity, the temperature difference between the target and the cone wall was responsible for 2.1C deviation from the target value.

The true emissivity and temperature of the target can be measured by using a cone heated at approximately the same temperature of the target. The temperature of the target can also be calculated by using an iterative method with the modified equation 10 and equation 4. A complete study using configuration factors for the cone/target geometry will be published in a future paper.

ACKNOWLEDGMENTS

The US Department of Energy supports the MTI satellite work at Sandia National Laboratories, Los Alamos National Laboratory and the Savannah River Technology Center. We appreciate the support of our colleagues at these laboratories and the support of the different private and public organizations working with us on MTI ground truth collections.

REFERENCES

1. M. Fuchs and C.B. Tanner: "Infrared Thermometry of Vegetation", *Agronomy Journal*, Vol. **58**:597-601 1966.
2. M. Fuchs and C.B. Tanner: "Surface Temperature Measurements of Bare Soils", *Journal of Applied Meteorology*, Vol. **7**:303-305 1968.
3. Bird, R. B., Stewart, W.E., and Lightfoot, E. N. Transport phenomena. John Wiley @ Sons, Inc., New York. 780p. 1965
4. Raymond J. Chandos and Robert E. Chandos "Radiometric Properties of Isothermal, Diffuse Wall Cavity Sources", *Applied Optics/ Vol. 13, No. 9, pages 2142, 1974*

Cone	Apex Diameter (cm)	Base Diameter (cm)	Height (cm)	Area Ratio (A_{apex}/A_{base})
Base	6.35	14.61	15.56	0.1890
C	3.30	14.61	23.18	0.0511
B	2.54	14.61	25.08	0.0302
A	2.03	14.61	25.72	0.0194

Table 1. Dimension of the cones used during the course of the experiment.

Tubular	Contact	Bare	Cone Base	Cone C	Cone B	Cone A
50.25	48.9	39.6				
50.08	49.44					47.3
50.07	49.39				46.9	
50.12	49.51			46.8		
50.14	49.46		44.3			

Table 2 shows the temperature of the target and with cones measured with the infrared radiometer, and the target temperature measured with the tubular thermometer and contact thermometer.

Target tubular temperature (C)	Target contact thermocouple temperature (C)	Radiometer Cone Temperature (C)	Radiometer Target Temperature (C)	Delta T (Contact-Radiometric Temperature)
21.57	21.39	21.5	21.7	-0.11
28.64	28.39	27.7	25.9	0.69
40.84	40.11	38.6	33.5	1.51
50.00	49.40	47.1	39.4	2.3
60.11	59.20	56.5	46.3	2.7

Table 3 shows a temperature dependent experiment and the temperature difference between the contact thermocouple and the radiometer with Cone A.

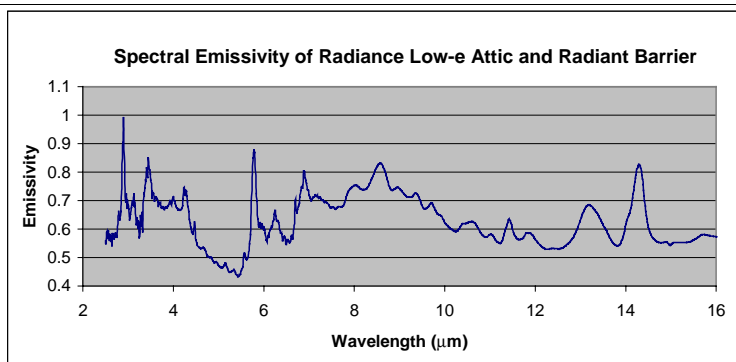
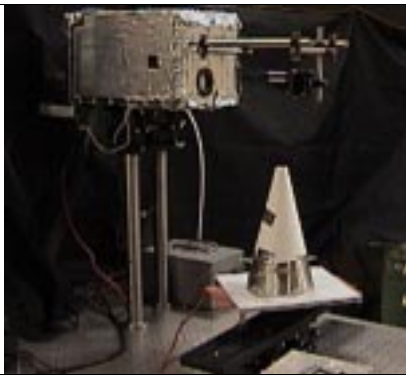


Figure 1 shows the FTIR looking at the heated target plate through cone A.

Figure 2. Spectral emissivity of Radiance Low-e Attic and Radiant Barrier

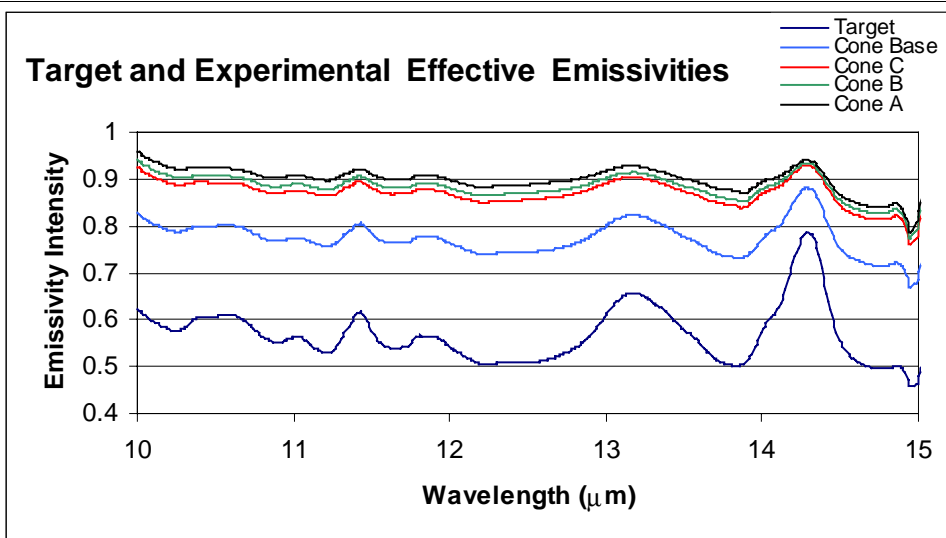


Figure 3. Spectral emissivity of Radiance Low-e Attic and Radiant Barrier and the respective effective emissivities with the different apex area cones.

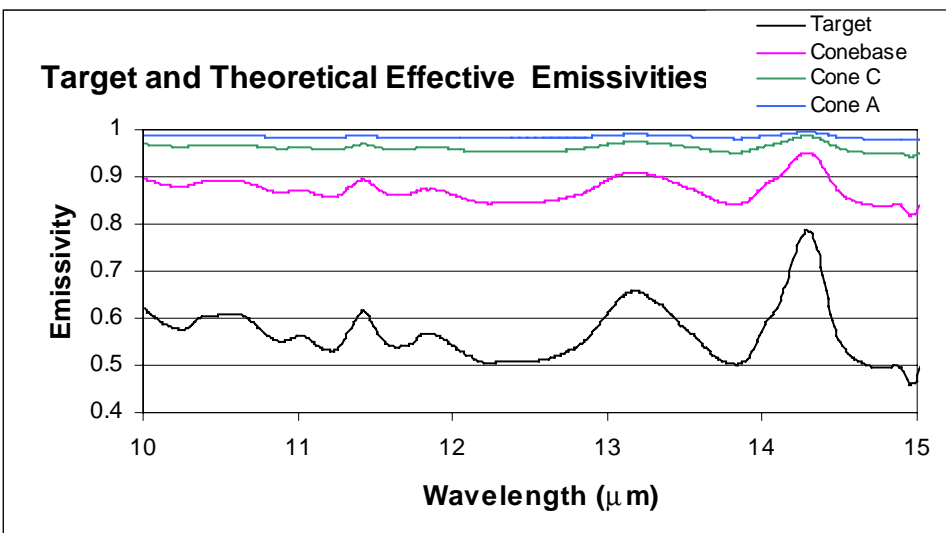


Figure 4. Theoretical spectral effective emissivity with the cones.

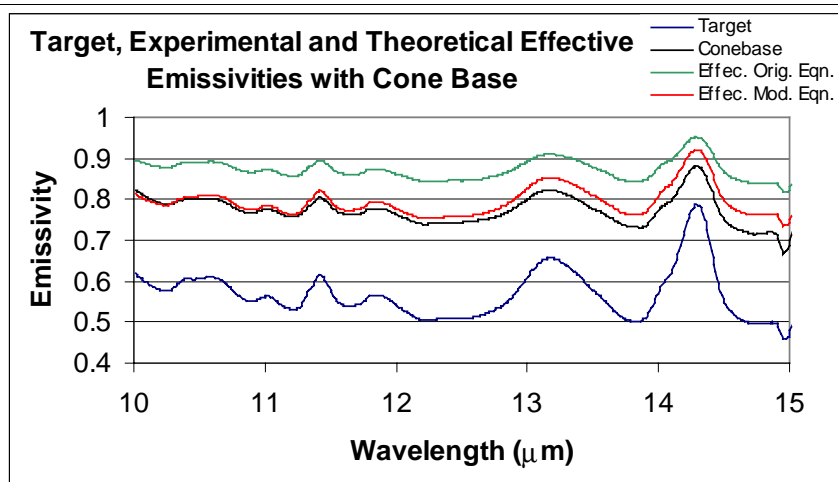


Figure 5a shows the target emissivity with the experimental effective emissivity with the conebase and the calculated effective emissivities using equation 2 and the modified version with energy exchange between the cone and the target.

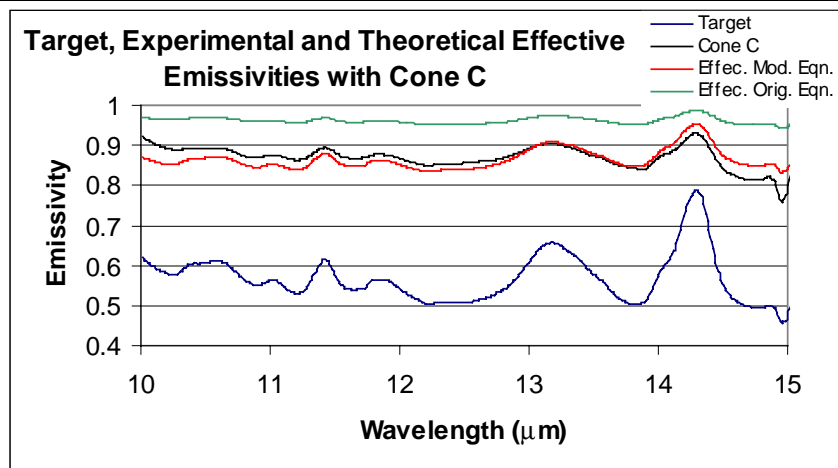


Figure 5b shows the target emissivity with the experimental effective emissivity with the cone B and the calculated effective emissivities using equation 2 and the modified version with energy exchange between the cone and the target.

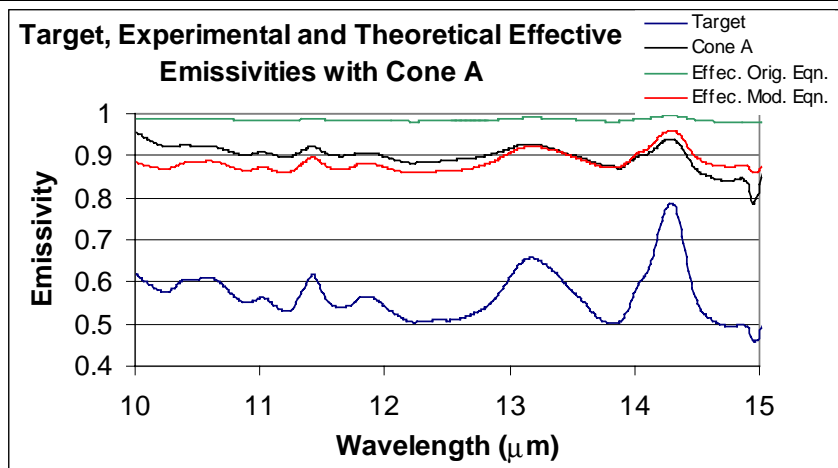


Figure 5c shows the target emissivity with the experimental effective emissivity with the cone A and the calculated effective emissivities using equation 2 and the modified version with energy exchange between the cone and the target.

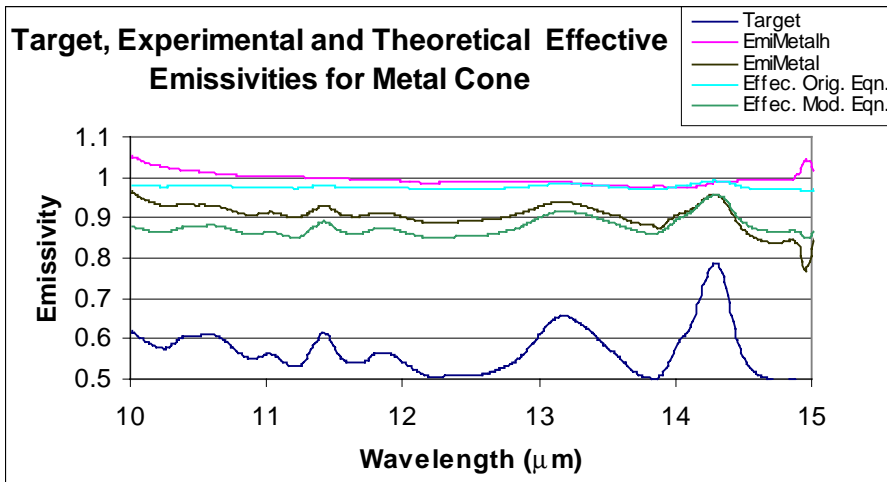
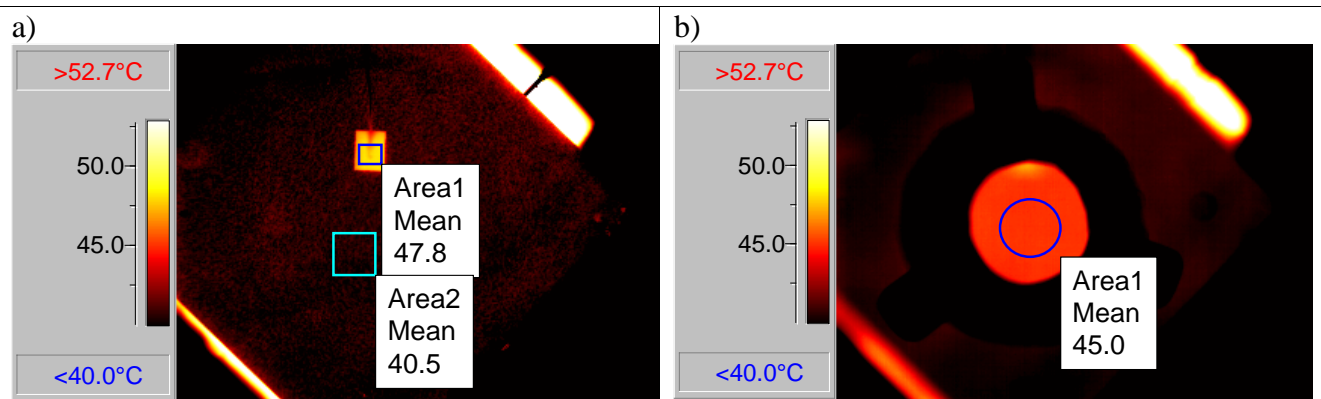
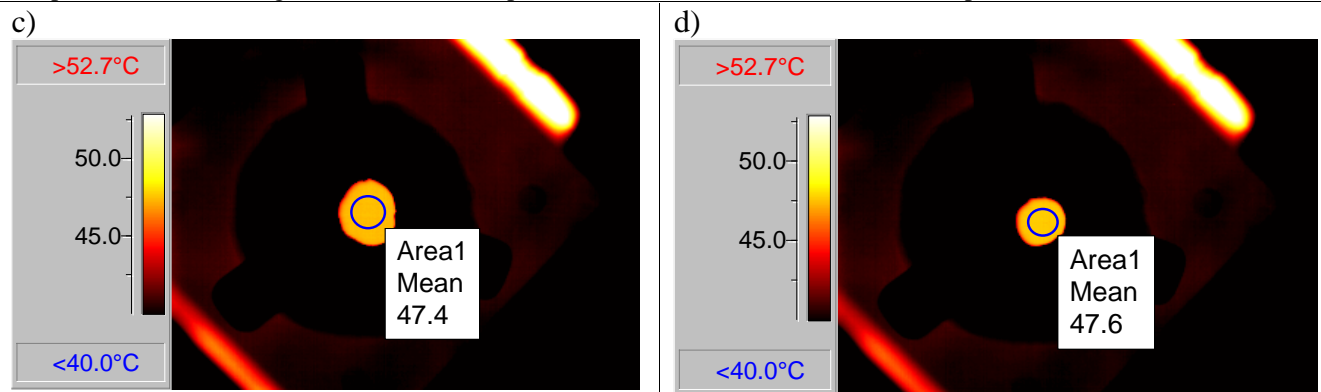


Figure 6 shows the target emissivity, the effective emissivity with metal cone (EmiMetal), the theoretical modified effective emissivity, the theoretical original effective emissivity and the experimental effective emissivity with a heated metal cone (EmiMetalh). The heated metal cone experimental emissivity and the theoretical effective emissivity calculated with equation 2 closely match.



Figures 7a shows the heated target plate imaged with an infrared camera. The average apparent temperature on the thermocouple is 47.8C. The average apparent target temperature is 40.5C. The higher emissivity of the contact thermocouple is evident in the image. Figure 7b show the cone base on top of the heated target plate. The average apparent temperature was observed to increase from 40.5C to 45C. Calibration of the radiometer indicates that temperatures are 0.8C higher than the true temperatures. See Table 2 for radiometric temperatures.



Figures 7c and 7d shows the effect on the apparent temperature of the target plate with cones A and B (different apex areas). Temperature readings are 0.8C higher than the true temperatures. See Table 2 for radiometric temperatures.